ACS APPLIED MATERIALS & INTERFACES

Research Article

www.acsami.org

Bulk Synthesis of Metal–Organic Hybrid Dimers and Their Propulsion under Electric Fields

Sijia Wang,[†] Fuduo Ma,[†] Hui Zhao,[‡] and Ning Wu*,[†]

[†]Department of Chemical and Biological Engineering, Colorado School of Mines, Golden, Colorado 80401, United States

[‡]Department of Mechanical Engineering, University of Nevada, Las Vegas, Nevada 89154, United States

Supporting Information

ABSTRACT: Metal–organic hybrid particles have great potential in applications such as colloidal assembly, autonomous microrobots, targeted drug delivery, and colloidal emulsifiers. Existing fabrication methods, however, typically suffer from low throughput, high operation cost, and imprecise property control. Here, we report a facile and bulk synthesis platform that makes a wide range of metal–organic colloidal dimers. Both geometric and interfacial anisotropy on the particles can be tuned independently and conveniently, which represents a key advantage of this method. We further investigate the self-propulsion of platinum-polystyrene dimers under perpendicularly applied electric fields. In 1×10^{-4} M KCl solution, the dimers exhibit both linear and circular motion with the polystyrene lobes facing toward the moving direction, due to the induced-charge electroosmotic flow surrounding the metal-coated lobes. Surprisingly, in deionized water, the same dimers move in an opposite direction, i.e., the metallic lobes face the forward direction. This is because of the impact of another type of electrokinetic flow: the electrohydrodynamic flow arising from the induced charges on the conducting substrate. The competition between the electrohydrodynamic flow along the substrate and the induced-charge electroosmotic flow along the metallic lobe dictates the propulsion direction of hybrid dimers under electric fields. Our synthetic approach will provide potential opportunities to study the combined impacts of the geometric and interfacial anisotropy on the propulsion, assembly, and other applications of anisotropic particles.

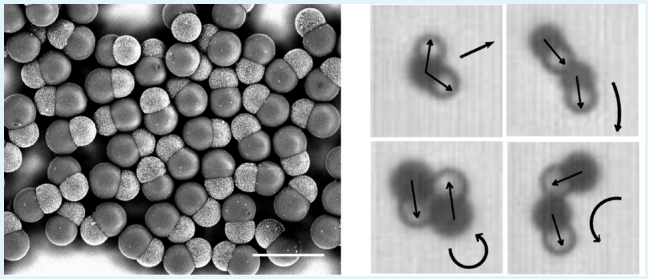

KEYWORDS: *anisotropic particle, induced-charge electroosmosis, electrohydrodynamics, electric field*

1. INTRODUCTION

Particles with anisotropic properties in geometry, interfacial functionality, or chemical composition have attracted a lot of attention recently because of their potential applications in self-assembly,[1] optical display,[2] emulsion stabilization,[3] molecular probes,[4] autonomous motors,[5] and drug delivery.[6] For example, gold nanorods with geometric anisotropy have been used as biomedical imaging agents due to their strong surface plasmon resonance at the near-infrared region.[7] When colloidal particles are functionalized with DNA patches, they behave similarly to the multivalent atoms and can self-assemble into a variety of colloidal molecules in a controllable fashion.[8]

Among different types of anisotropic particles, the metal–organic hybrid particles[9] are of special interest because (1) the interfacial properties on the metallic and organic regimes can be conveniently tailored due to their complementary difference in surface chemistry and (2) they combine unique properties from both metallic and organic materials such as the electric conductivity, catalytic activity, plasmonic property, etc. The asymmetric interfacial properties can also be utilized to induce autonomous motion of hybrid particles in aqueous solutions based on a number of different mechanisms.[10−13] For example, a platinum-polystyrene sphere[14] can move actively in hydrogen peroxide solutions due to the so-called self-diffusiophoresis.[15] The platinum-coated hemisphere catalyzes the decomposition of hydrogen peroxide, whereas the polystyrene hemisphere remains inert. As a result, there is a concentration gradient of oxygen surrounding the particle, which generates solvent flow and propels the particle. In addition to the difference in catalytic activity, metallic and polymeric materials have distinguished electric polarizabilities. For example, gold–polystyrene Janus spheres can move laterally under a perpendicularly applied AC electric field,[16] because of the so-called induced-charge electroosmosis (ICEO).[17,18] The external electric field polarizes the metallic hemisphere and induces mobile ions in the diffusive layer, which move under the applied field and generate a net fluid flow toward the gold-coated part. Previous studies, however, were mostly focused on Janus spheres, which is still symmetric in shape. The combined impacts of geometric and interfacial anisotropy on the self-propulsion of particles remain elusive at this moment.

This is partially because it is challenging to fabricate metal–organic particles in high throughput with narrow polydispersity, which is crucial for practical applications. Conventional

Received: January 19, 2014
Accepted: March 2, 2014
Published: March 3, 2014

   dx.doi.org/10.1021/am500398p | ACS Appl. Mater. Interfaces 2014, 6, 4560–4569

strategies[12−16] often rely on templating methods by first depositing a monolayer of particles on a flat substrate. A thin metallic film is then deposited on the particle array via thermal or electron-beam evaporation. Due to the shadowing effect, the top surface of the particles is coated with metal while the bottom half stays intact. This technique is inherently two-dimensional and is associated with low throughput and high operational cost. A three-dimensional templating method based on Pickering emulsion, in principle, could produce large quantities of hybrid particles.[19,20] However, it is usually restricted to spherical particles with carefully tailored surface properties in order to form Pickering emulsions. The geometric and interfacial anisotropy cannot be modulated independently. Controlled heterogeneous nucleation and growth[21−24] have also been developed for making metal−organic particles. But they are either too small[25,26] for in situ observation through optical microscopy or hard to control the morphologies precisely.[22,27,28] Facile synthetic strategy to make microscopic metal−organic particles with tunable anisotropy in both geometry and interfacial properties is still missing.

In this paper, we report a bulk synthesis approach to make different types of metal−organic hybrid dimers with independent control of the geometric and interfacial anisotropy. We further investigate the self-propulsion of those dimers under electric fields. Modified from previously developed seeded-emulsion polymerization,[29−37] we make polystyrene dimers with well-controlled geometric anisotropy that can be characterized by the size ratio between two lobes and bond length. The incorporation of functional silanes during the synthesis stage allows us to combine the sol−gel chemistry[38]and amine-metal complexation[39,40] to grow a variety of metallic films on one of the two lobes selectively. Two key advantages of this synthetic route are that (1) we can systematically tune the geometric and interfacial anisotropy between two lobes in an independent and precise fashion, and (2) it produces hybrid particles with high throughput and reasonable monodispersity. We have also investigated the self-propulsion of the platinum-polystyrene dimers under electric fields. In higher salt concentrations (e.g., 1×10^{-4} M), we find that the dimers propel with the dielectric lobes facing the forward direction, primarily due to the induced-charge electroosmosis surrounding the metallic lobe. At lower salt concentrations (e.g., in deionized water), however, they move with the metallic lobes orienting in the propulsion direction, because of stronger electrohydrodynamic flow along the polystyrene lobe. Moreover, the propulsion speed of a hybrid dimer is very sensitive to its orientation, which can be conveniently tuned by the frequency. Our studies reveal important impacts of the combined geometric and interfacial anisotropy on the electric-field driven propulsion of colloidal particles.

2. EXPERIMENTAL METHODS

Materials. Styrene, divinylbenzene (DVB), sodium 4-vinylbenzenesulfonate, polyvinylpyrrolidone (PVP, $M_w \approx 40\,000$), sodium dodecyl sulfate (SDS), 3-aminopropyltriethoxysilane, and L-ascorbic acid are purchased from Sigma-Aldrich. 3-(trimethoxysily)propyl acrylate (TMSPA) is purchased from TCI. Hydrogen tetrachlororaurate(III) trihydrate ($HAuCl_4 \cdot 3H_2O$, 99.9+%), silver nitrate ($AgNO_3$, 99.9+%), and potassium tetrachloroplatinate(II)-(K_2PtCl_4, 99.9%) are bought from Alfa Aesar. The thermal initiator V65 is bought from Wako Chemicals. All chemicals are used as received except that both styrene and divinylbenzene are purified by aluminum oxide before usage.

Synthesis of Polystyrene (PS) Dimers. The synthetic route we use to make colloidal dimers is based on a modification of the methods of Sheu and Kim.[28−36] Typically, spherical PS seed particles are first prepared by the dispersion polymerization in methanol[41] and are cleaned four times via centrifugation (4000 rpm, 30 min, IEC HT Centrifuge). After that, a mixture of 4 mL of 5 wt % PVP aqueous solution, 0.5 mL of 2 wt % SDS, 1 mL of styrene, 0.05 mL of DVB, 0.05 mL of functional silanes (such as 3-trimethoxysily propyl acrylate), and 0.02 g of V65 is emulsified using ultrasonication (Branson digital sonifier 450). The emulsion is then used to swell 1 mL of polystyrene seed particles (10 wt % in deionized water) for 24 h. The swollen seeds are then polymerized and cross-linked in the reactor at 70 °C for another 24 h. PS dimers are synthesized via a second swelling stage. Again, we use styrene (with variable amount to control the size of the second lobe) to swell 1 mL cross-linked PS seeds (1 wt %) with 4 mL 5 wt % PVP, 0.5 mL 2 wt % SDS, and 2 wt % V65. Subsequently, polymerization is performed at 70 °C for 24 h. The synthesized dimers are then cleaned four times via centrifugation.

Selective Coating of Gold Nanoparticles on the Cross-Linked Lobe. During the synthesis of the cross-linked spherical seed particles, different types of functional silane molecules are incorporated in the particles to control the bond length of the dimers. In addition, those silane molecules remain in the cross-linked lobe, which allows us to further attach (3-aminopropyl)-triethoxysilane (APS) on it via the silane coupling chemistry. For example, we mix 0.02g dimers in 15 mL ethanol solution with 100 μL APS and 3 mL ammonia hydroxide (30% NH_4OH) and stir the mixture for 24 h at the room temperature.[39] The particles are then washed by ethanol for four times and redispersed in water. Once the dimers are functionalized with APS, we mix them with citrate-stabilized gold nanoparticle solutions (Turkevich method[42]) in a sonication bath for 1 h. We then use Track-etched filter papers (Whatman) to completely remove free gold nanoparticles that are suspended in the solution.

Gold/Silver and Platinum Shell Growth on Gold-Coated Dimers. To coat an additional layer of gold/silver, we mix 4 mL gold-coated dimers (0.1 wt %) with 0.4 mL 30 mM $HAuCl_4 \cdot 3H_2O/AgNO_3$ by sonication for 10 min. Then 70 μL formaldehyde is added in the solution, while stirring for 10 min. One milliliter of NH_4OH (0.3%) is added within 2 min afterward. The solution is kept stirring for 1 h and allowed standing for another hour. For the shell growth of platinum, we mix 1 mL gold-coated dimers ($\sim 1 \times 10^8$ particles/ml) with 0.3 mL 100 mM freshly prepared ascorbic acid solution, followed by adding 2 mL 2 mM K_2PtCl_4 within one hour. If a thicker and more uniform coating is desired, one can recoat the dimers with 0.3 mL of 100 mM ascorbic acid and 2 mL of 2 mM K_2PtCl_4 solutions without stirring. Two-step coating is necessary because if a higher concentration of platinum salt is used (e.g., 5 mM K_2PtCl_4), we lose the capability to coat platinum anisotropically on one lobe only.

Characterization of the Hybrid Dimers. The surface morphologies of hybrid dimers are characterized by scanning electron microscopy (JEOL JSM-7000F). The element compositions of both lobes are analyzed by the energy-dispersive X-ray (EDX). An inverted microscope (Olympus IX71) is used for bright-field and fluorescent imaging.

Propulsion of Pt-PS Dimers under Electric Fields. After synthesis, the Pt-PS dimers are first cleaned four times using centrifugation. They are then dispersed in 1×10^{-4} M potassium chloride (KCl) solution or in deionized water. The dimers are then injected into the chamber formed by two pieces of indium−tin-oxide (ITO) glasses with an insulating spacer (~100 μm in thickness) to control the separation between top and bottom electrodes. After dimers settle down to the bottom substrate, an AC electric field is applied (RigolDG1022). A high speed camera (SILICON VIDEO monochrome SV642) is used to record the motion of dimers at 30 frames/s for at least 30 s. We then use ImageJ[43] to track the dimers' movement and obtain their instantaneous positions. Two different methods have been employed to obtain the average velocities of the dimers. As shown in the Supporting Information, Figure S1a, the accumulative displacement of a dimer is plotted vs time. The average velocity is then calculated from the slope. This method, in principle,

works the best when the trajectory is unidirectional and the propulsion velocity is much faster than the Brownian motion. We have also employed a second method that was first proposed by Howse et al.[14] Shown in the Figure S1b in the Supporting Information, the mean square displacement (MSD) $\langle \Delta L^2 \rangle$ is plotted as a function of time. When Δt is much less than the inverse rotational diffusion coefficient of the dimer τ_R, the curve can be fitted[14] with a quadratic function of Δt

$$\langle \Delta L^2 \rangle = v^2 \Delta t^2 + 4 D_e \Delta t \quad (1)$$

where v and D_e are the propulsion speed and the effective (two dimensional) diffusion coefficient of a dimer, respectively. We confirm that both methods yield very similar propulsion velocities.

3. RESULTS AND DISCUSSION

Synthesis of the Metal–Organic Hybrid Dimers. Figure 1 illustrates our overall strategy to synthesize the metal–organic

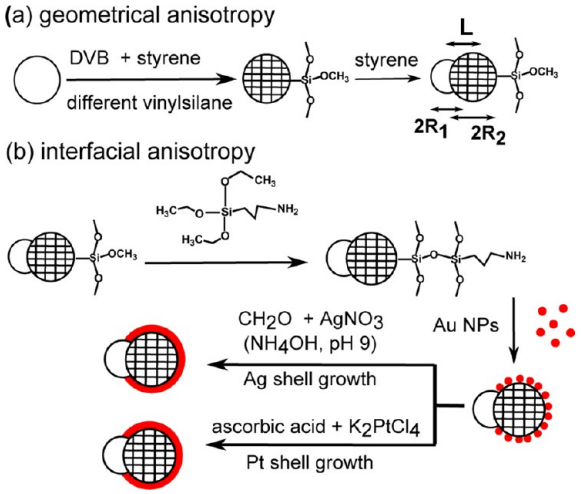

Figure 1. Chemical route to synthesizing metal–organic hybrid dimers with independently tunable (a) geometric and (b) interfacial anisotropy.

hybrid dimers with independently tunable geometric and interfacial anisotropy. Polystyrene dimers are first synthesized via the seeded emulsion polymerization.[29−37] In brief, spherical polystyrene particles are first cross-linked by adding styrene, divinylbenzene, and different types of functional vinylsilanes. The cross-linked seeds are then swollen with styrene again, where the elastic contraction of the cross-linked polystyrene expels styrene out of the swollen seeds and gives rise to a second lobe. To increase the stability of dimers in water, we have also added comonomer sodium 4-vinylbenzenesulfonate so that the dimers are negatively charged. As shown in Figure 1, both size ratio $\alpha = R_1/R_2$ and the dimensionless bond length $\beta = L/(R_1 + R_2)$ are important parameters to characterize the geometric anisotropy.

The size ratio α can be controlled by adjusting the relative amount of styrene to the cross-linked seed particles (CPS) during the second swelling stage. As shown in Figure 2a, the second lobe diameter increases with increasing amount of styrene while CPS (i.e., the original lobe) does not change its size significantly. We have also found that the incorporation of functional vinylsilanes during the synthesis of CPS has a significant impact on the bond length due to different compatibility between silane molecules and styrene. Shown in Figure 2b, when the functionality in the silane molecule

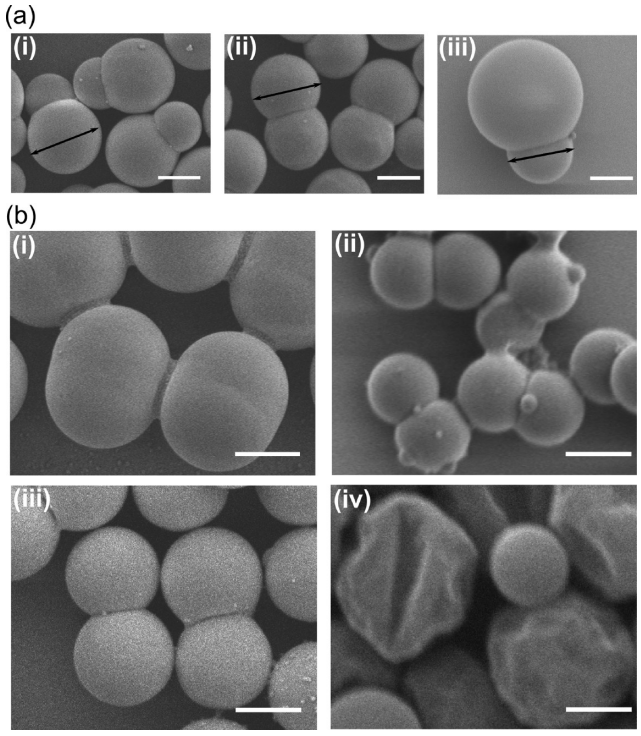

Figure 2. (a) Size ratio between two lobes $\alpha = R_1/R_2$ can be tuned by changing the amount of styrene used to swell the cross-linked particles. The black arrow represents the seed particle, i.e., the original lobe. (b) The dimer bond length $\beta = L/(R_1 + R_2)$ is sensitive to the type of functional vinylsilanes added in the cross-linked seeds: (i) no silane (β = 0.3); (ii) styrylethyltrimethoxysilane (β = 0.7); (iii) trimethoxysilylpropylacrylate (β = 0.84); (iv) methacryloxypropyltrimethoxysilane (β = 1). Scale bar for all images: 1 μm.

changes from styrene to acrylate, the bond length β increases due to an enhanced phase separation during the polymerization of the second lobe. In the case of methacryloxypropyltrimethoxysilane, styrene barely swells the CPS and the bond length is approximately one, indicating poor compatibility between methacrylate and styrene. This poor compatibility could make the CPS surface more hydrophilic, hence increasing the bond length between the two lobes.[44] In addition to its impact on the geometric anisotropy, the incorporation of functional silanes in CPS also allows us to create interfacial anisotropy conveniently. For example, we can attach (3-aminopropyl)-triethoxysilane (APS) on the cross-linked lobe using the silane coupling chemistry.[38] The attachment of APS can be confirmed by the fluorescence image in Figure 3b, where neutral fluorescein

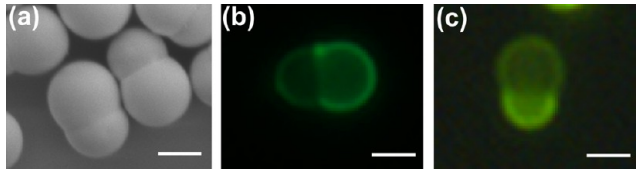

Figure 3. (a) A SEM image of dimers in which the larger lobe is coated with (3-aminopropyl)-triethoxysilane. (b) The fluorescent image of the same dimer after it is coated with neutral FITC dye, which couples strongly with amine groups on the larger lobe. (c) The fluorescent image of the same dimer after it is coated with positively charged rhodamine 6G, which can absorb on negatively charged surfaces. Scale bar for all images: 1 μm.

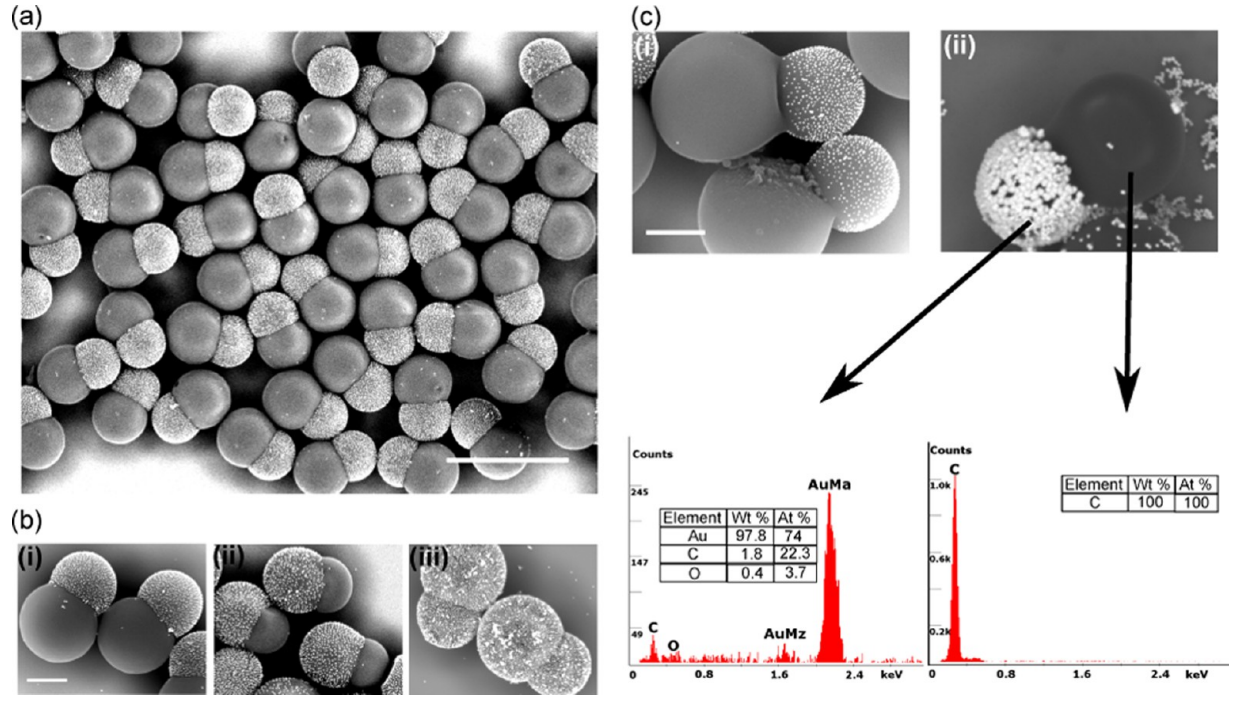

Figure 4. (a) Large field of view of gold-polystyrene hybrid dimers where the brighter lobe is coated with gold nanoparticles. Scale bar: 4 μm. (b) Gold nanoparticles can be selectively coated on either (i) smaller or (ii) larger lobes as long as it is functionalized with APS. (iii) When both lobes bear APS, gold nanoparticles are coated uniformly. Scale bar: 1 μm. The scale bar is same for i, ii, and iii. (c) Surface coverage of gold can be significantly enhanced through (ii) a second nucleation and growth stage on (i) the Au-PS hybrid dimers, as evidenced by the element analysis using EDX. Scale bar: 1 μm. The scale bar is same for both i and ii.

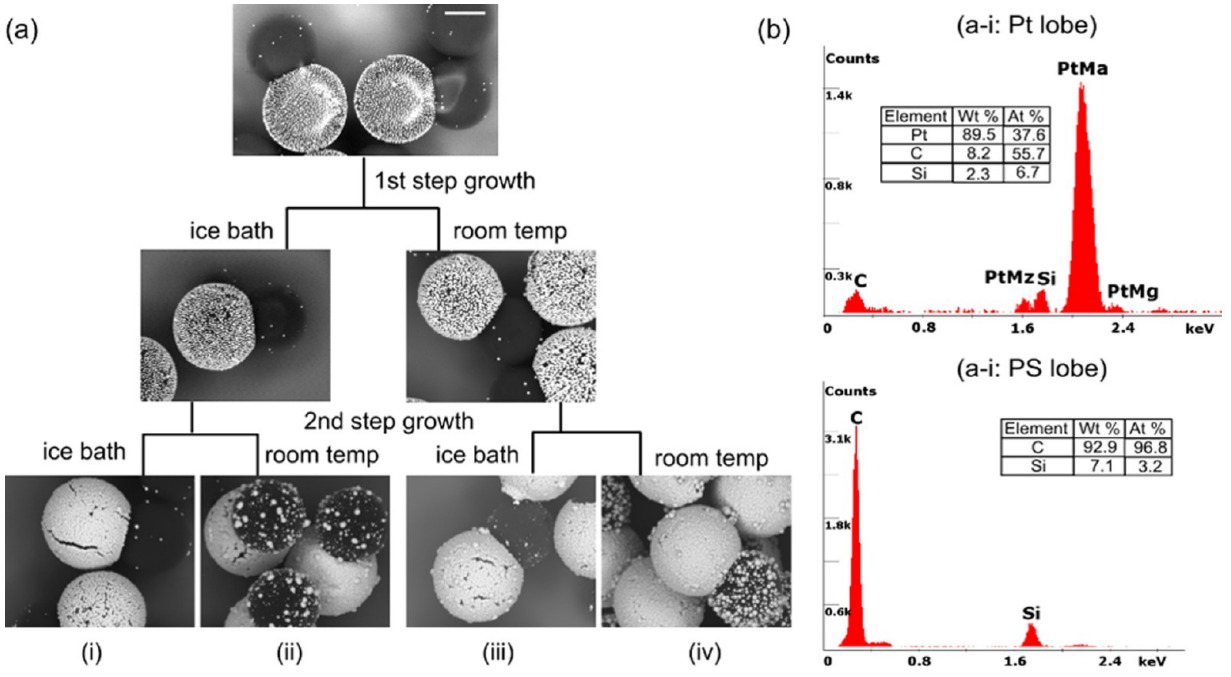

Figure 5. (a) Effect of deposition temperature on the surface coverage of the platinum coating. Two-step growth made more uniform and denser coating of platinum if the conditions are correct, e.g., i and iii. Scale bar: 1 μm. The scale bar is same for all images. (b) The EDX analysis on the platinum-coated and polystyrene lobes. The Si signal arises from the silicon substrate used for preparing SEM samples.

isothiocyanate (FITC) are selectively bonded to the amine groups on the original (large) lobe via the isothiocyanate-amine reaction.[33] Alternatively, when we mix dimers with a positively charged dye rodamine 6G, a stronger fluorescent intensity is observed on the second (smaller) lobe because the amine groups partially neutralize the negative charges on the original lobe (Figure 3c).

Since amine groups form complexes with metals, we can further coat a thin layer of presynthesized gold nanoparticles (~20 nm) selectively on the lobe with APS functionalization, as shown in images a and b in Figure 4. As a comparison, the

dx.doi.org/10.1021/am500398p | ACS Appl. Mater. Interfaces 2014, 6, 4560−4569

control experiment show nondiscriminating coating (Figure 4b-iii) on dimers with APS functionalization on both lobes. The surface coverage of gold nanoparticles can be further enhanced by mixing the Au-PS dimers with chloroauric (Au^{III}) acid and formaldehyde (Figure 4c). The additional reduction of gold ions (by formaldehyde) on the seeded gold nanoparticles creates more uniform and dense coating on the hybrid dimers, as evidenced by both SEM images and the energy-dispersive X-ray spectroscopy (EDX) results in Figure 4c.

The gold nanoparticles on hybrid dimers could be utilized as heterogeneous nucleation sites to promote selective coating of other metals, such as silver and platinum. The former is an excellent material for plasmonic properties[45] while the latter is an important catalyst. By suspending Au-PS dimers in silver nitrate solution and using formaldehyde[46] or hydroxylamine hydrochloride[39] as the reducing agent, we can grow a silver shell with thickness ~100 nm anisotropically (see the Supporting Information, Figure S2). We have found that the proper control of the redox speed is critical for selective coating of silver. Homogeneous nucleation of silver in solution can be suppressed by choosing a milder reducing agent (e.g., formaldehyde), limiting the maximal salt concentration (<5 mM), and adding ammonia hydroxide dropwise to carefully control the solution pH.

We can adopt a similar strategy to grow a platinum shell on the dimers although a milder reducing agent than formaldehyde is necessary. Otherwise, black precipitates would form within five minutes even at neutral pH. Therefore, we choose ascorbic acid as the reducing agent.[47−49] With properly adjusted pH, reaction temperature, and the concentration ratio between dimers and metal salts, we have successfully achieved a selective coating of platinum, as shown in Figure 5a. Although keeping lower ascorbic acid concentration helps maintaining the anisotropic coating due to a lower reaction speed, its concentration needs to be high enough to ensure good colloidal stability during the shell growth. However, this limited redox speed prevents platinum from coating a complete shell in one step. Therefore multiple growth steps are necessary for dense coating. Although both room and low temperatures (e.g., ice bath) yield satisfactory coatings on the selected lobe during the first step (Figure 5a), low temperature is necessary in the second growth step to reduce the extent of platinum deposition on the other lobe (Figure 5a-ii and iv).

In summary, we have developed a versatile and bulk-synthesis strategy to make metal−organic hybrid dimers with tunable geometric and interfacial anisotropy. We demonstrate our concept by three types of metallic coatings: gold, silver, and platinum, and it should be readily extended to other types of inorganic materials too. Compare with the commonly used templating methods for making Janus spheres,[11,12,14] our bulk-synthesis strategy has the great potential for high throughput and low cost. Moreover, the combined asymmetry in both geometric shape and interfacial property on our dimers allows us to investigate its impact on the self-propulsion of microparticles in a fluidic environment. In the following, we will report the electric-field driven propulsion of platinum-polystyrene dimers.

Propulsion of Hybrid Dimers under AC Electric Fields. The synthesized Pt-PS dimers are first dispersed in deionized water. An appropriate amount of salt (e.g., potassium chloride) are then added to control the Debye length. As illustrated in Figure 6, ~10 μL of the solution is injected into a chamber sandwiched by two conducting substrates. After the dimers settle down, a square AC bias 5−20 V_{pp} is applied between top and bottom electrodes. We first examine the propulsion of hybrid dimers in 1×10^{-4} M salt water. At ~2 kHz, dimers align parallel to the substrate (i.e., lying dimers) except a few are perpendicular (i.e., standing dimers). We find that all lying dimers move horizontally, while both standing dimers and uncoated polystyrene dimers only exhibit Brownian motions (see the Supporting Information, Movie 1). We also notice that a moving dimer always orients its polystyrene lobe toward the propelling direction, as shown in Figure 7a. On the basis of the recorded images, we can calculate the propulsion velocities at different field strengths and frequencies. Shown in Figure 7b, the velocity of lying dimers scales well with the square of the field strength, i.e., $u \propto E_0^2$, whereas the other dimers move Brownianly. Figure 7c reports the dependence of the velocity on frequencies. The curve peaks at an intermediate frequency ~2 kHz and decays when the frequency is decreased to zero or increased beyond a few kilohertz.

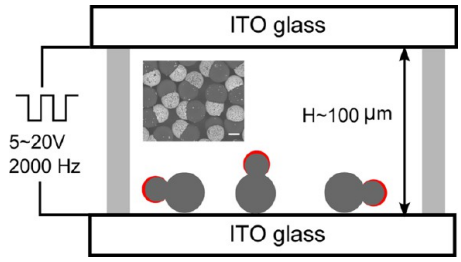

Figure 6. Schematic of our experimental setup for dimer propulsion under external AC electric fields. The red represents the platinum coating.

Although the dimers in Figure 7a move with its polystyrene lobe pointing forward, the dielectric lobe (~1.9 μm) is also larger than the platinum-coated lobe (~1.7 μm). We have also tested two other batches of hybrid dimers where the platinum-coated lobe is approximately equal to or larger than the bare polystyrene lobe. As shown in Supporting Information movie 2, both types of dimers propel with the polystyrene lobe oriented forward, regardless of their relative sizes. Their velocities also scale with the square of the applied field (see the Supporting Information, Figure S3).

Our observations so far can be explained under the theory of the induced-charge electrophoresis.[17,18] As shown in Figure 7d, the platinum-coated lobe is much more polarizable than the bare polystyrene lobe because of the metallic conductivity. Under AC fields, the polarized platinum lobe induces diffusive charges surrounding it. Those ions can respond to the applied field and generate the so-called "induced-charge electroosmotic (ICEO)" flow of solvent from the pole to the equator of the particle. While Figure 7d only illustrates the solvent flow during one-half period of the AC field, the flow direction does not change during the second half period because both the applied field and the induced-charges will change their signs. For a metallic sphere, the quadrupolar solvent flow does not generate a net movement of the particle because of the symmetry. But for Pt-PS dimers, the ICEO flow is much stronger along the platinum-coated lobe than the dielectric (polystyrene) lobe. Such a broken symmetry[18] in the interfacial polarizability induces the propulsion of dimers along the long axis, i.e., the x-direction. Therefore, the hydrodynamic shear will push the dimer with its dielectric lobe oriented forward, regardless of its relative sizes. This directional movement is consistent with both ICEO theory[18] and experiments for Janus spheres.[16] The

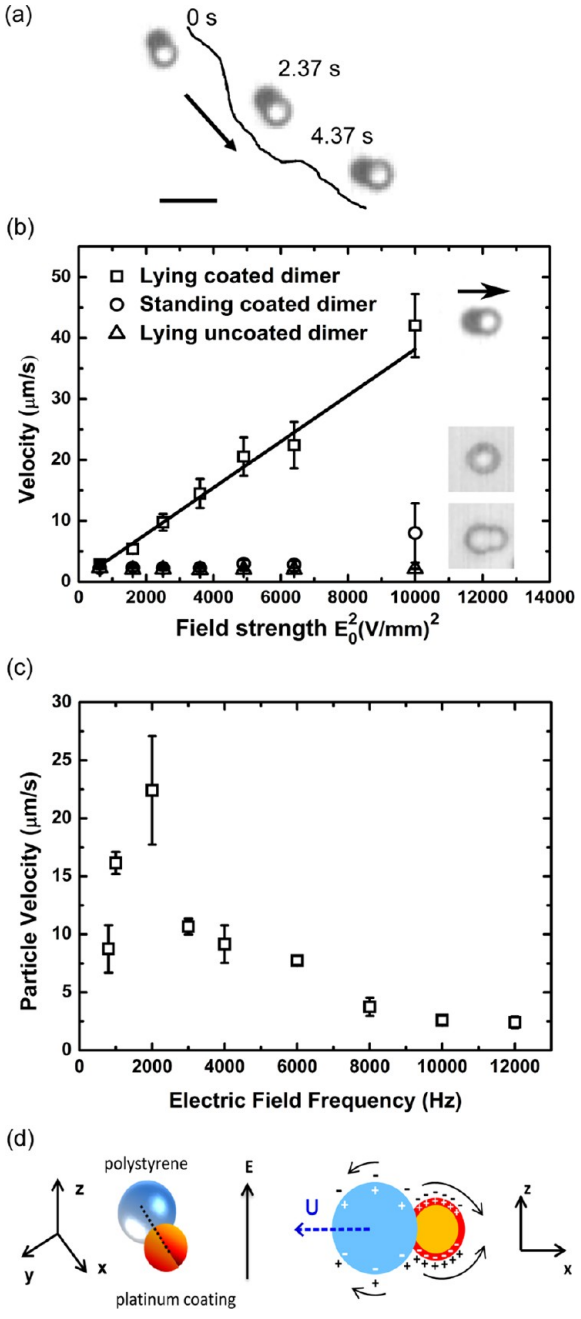

Figure 7. (a) Linear motion (100 V_{pp}/mm, 2 kHz) of Pt-PS dimers. Several optical snapshots show the dimer's orientation at different time. The dark sphere represents the platinum-coated lobe, and the bright sphere is the polystyrene lobe. Scale bars: 10 μm. The dimer itself is about 2 μm. (b) The propulsion velocity (at 2kHz) of lying Pt-PS dimers (square), standing Pt-PS dimers (circle), and lying uncoated PS dimers (triangle) at different field strengths in 1×10^{-4} M KCl solutions. The arrow indicates the propulsion direction. The platinum-coated lobe (R_1 = 0.85 μm) is smaller than the dielectric lobe (R_2 = 0.95 μm). (c) Propulsion velocity of the lying Pt-PS dimers at different frequencies (1×10^{-4} M KCl and 14 V_{pp}). (d) Polarizability difference between the platinum-coated and polystyrene lobes generates an ICEO flow that propels the dimer laterally with its polystyrene lobe oriented along the forward direction. The x–y plane is parallel to the bottom substrate, and the electric field is applied in the z-direction.

frequency dependence of the propulsion velocity is also expected. When the frequency is below the inverse of the charging time for the electrode τ_e, a fully developed diffusive layer will polarize the electrode. As a result, the electric field in the bulk and surrounding the particle is small.[17] Therefore, the ICEO velocity is low. When the frequency is beyond the inverse of the charging time for the metallic lobe τ_p, there is no enough time for the formation of the induced-charge screening clouds, which also makes the ICEO disappear. Therefore, dimer propulsion only exists in a frequency regime between τ_e^{-1} and τ_p^{-1}. Those two charging times are related to the Debye length κ^{-1}, the electrode separation H, the particle size R, and the diffusivity of ions D, i.e., $\tau_e = \kappa^{-1}H/D$ and $\tau_e = \kappa^{-1}R/D$, respectively.[17] Substituting our experimental conditions, we found that τ_e is ~700 Hz and τ_p is ~70kHz. Neglecting its frequency dependence, the ICEO velocity can be expressed.[16]

$$U_{ICEO} = \frac{9}{64}\frac{R}{1+\delta}\frac{\varepsilon\varepsilon_0 E_0^2}{\mu} \quad (2)$$

where ε is the dielectric constant of the solvent, ε_0 is the permittivity of the vacuum, μ is the solvent viscosity, and δ is the ratio of the differential capacitances between the compact and diffuse layers. We obtain $\delta \approx 20$ by fitting the curve in Figure 7b.

Once understanding the propulsion mechanism of individual hybrid dimers, we will be able to predict the moving directions of multiple dimers that form into clusters. Those clusters possess higher order of broken symmetry, which can exhibit more controllable propulsion behavior. A few examples are summarized in Figure 8 and displayed in the Supporting Information, Movie 3.

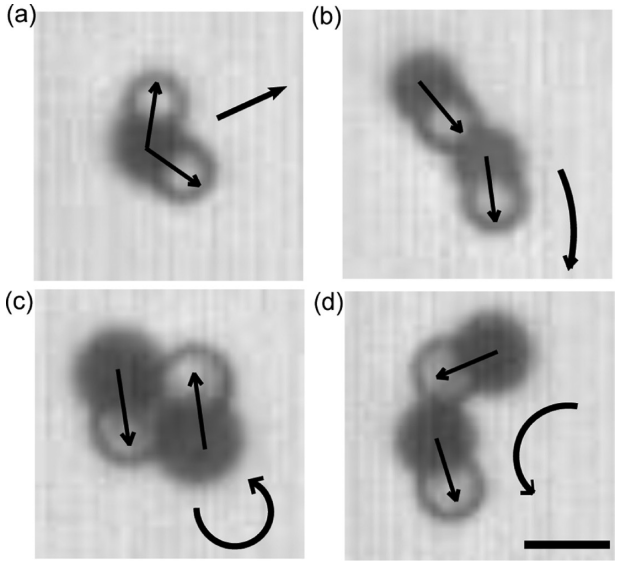

Figure 8. Propulsion of several types of dimer clusters: (a) two dimers sharing one metallic lobe; (b) head-to-tail dimer doublets with obtuse angle; (c) head-to-tail dimer doublets with zero angle; (d) head-to-tail dimer doublets with right angle. The individual arrow on each dimer shows its specific propulsion direction. The arrow outside shows the propulsion direction of the cluster.

Our chemically synthesized Pt-PS dimers, unlike Janus spheres, are anisotropic in both geometry and interfacial property. This combined anisotropy has profound impacts on the propulsion of particles that have not been observed before. For example, previous studies[16] mainly reported linear motions because the metal film was E-beam evaporated uniformly on one-half surface of the polystyrene spheres. We, however, have

dx.doi.org/10.1021/am500398p | ACS Appl. Mater. Interfaces 2014, 6, 4560–4569

observed both linear and circular motions for our dimers (see SI movie 4, Figure 7a, and Figure 9a). This circular motion

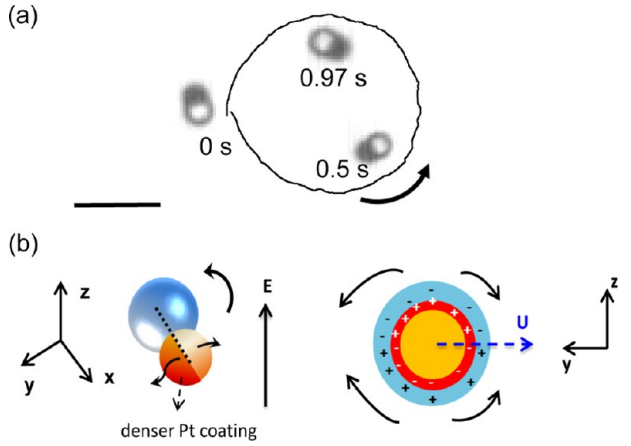

Figure 9. (a) Circular motion of dimers (200 V_{pp}/mm, 2 kHz). Scale bars: 10 μm. (b) The rotation could be attributed to the nonuniform coating of platinum on the smaller lobe.

could be attributed to potentially nonuniform platinum coating on the lobe. As depicted in Figure 9b, if one hemisphere of the small lobe has slightly denser coating than the other half, asymmetric ICEO flow along the *y*-direction could be generated. Different from the ICEO flow in *x*-direction, the *y*-direction flow is perpendicular to the dimer's long axis. Therefore, a torque would be generated, which makes the dimer move counterclockwise, as shown in Figure 9b. Because of the chemical deposition method employed here, the platinum coating on the smaller lobe is far from perfectly uniform, as can be seen clearly in Figure 5. Even a slight imbalance on the uniformity between left and right hemispheres could cause the circular motion. In fact, we observe equal populations of clockwise and counterclockwise motions due to the stochastic nature of coating. This ICEO flow in the *y*-direction is, however, a secondary effect compared with the ICEO flow in the *x*-direction, which arises from the anisotropy in polarizability between metallic and dielectric lobes. Therefore, the circular motion is manifested more significantly at higher field strengths. Even when dimers undergo the circular motion they still keep their orientations with the dielectric lobe pointing forward, again because the primary and strong ICEO flow is along the *x*-direction.

After confirming the behavior in high salt concentration, we also investigate the self-propelling of Pt-PS dimers at a much lower salt concentration (i.e., in deionized water). The behavior of our dimers in DI water is somehow surprising. First, about 50% of the lying dimers orient to the opposite direction now, i.e., the platinum-coated lobe orients toward the propelling direction (see the Supporting Information, Movie 5). When we plot the velocity vs the field strength, it still scales with E_0^2 (Figure 10a). Second, although the rest of the dimers still orient in the same direction that is predicted by the ICEO theory (i.e., the polystyrene lobe faces forward), the speed reduces dramatically. This is unexpected since the ICEO velocity should remain almost unchanged when the salt concentration is reduced.[16,50] Last but not the least, the frequency dependence is very different from our previous results in 1×10^{-4} M salt solution. As shown in Figure 10b, the particle velocity decreases monotonically when the frequency is increased within a narrow

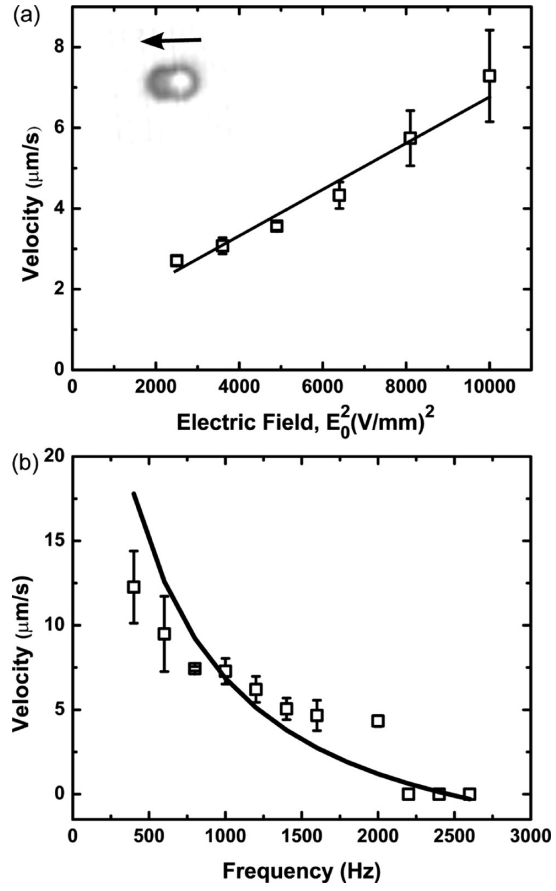

Figure 10. (a) Velocity of Pt-PS dimers in DI water (16 V_{pp} and 2 kHz). They orient the metallic lobes toward the propulsion direction, opposite to Figure 8. (b) Frequency dependence of the velocity. The solid curve is the theoretical prediction based on eqs 2 and 3 with $f \approx 0.0055$.

range. It stops moving beyond ~2 kHz where the lying dimers essentially align parallel with the direction of the applied field, i.e., they stand on the substrate (see the Supporting Information, Movie 5). Clearly, the speed of a colloidal dimer, which is anisotropic in geometry, also depends on its orientation. This provides us another degree of freedom to control the propulsion of particles.

Because our results cannot be solely explained by the induced-charge electroosmosis surrounding the platinum-coated lobe, there must exist a second type of flow which can also propel the particles. Here, we argue that the electrohydrodynamic flow (EHDF) along the conducting substrate can compete with the ICEO and propel our dimers into the opposite direction under right experimental conditions. The EHDF on a conducting substrate was first proposed by Trau, Ristenpart, Aksay, and Saville.[51−54] Under applied electric fields, an excess amount of surface charges can be induced within the diffusive layer near the conducting substrate. Although the external field is perpendicular to the substrate, the polarization of the particle distorts its local field and creates a tangential component that is parallel to the substrate. This tangential field acts on the induced charges and causes an EHDF along the substrate. In fact, this flow can be strong enough to entrain all neighboring particles and to form close-packed aggregates.[51] For spherical particles with isotropic surface properties, the EHDF is symmetric. This symmetry can

dx.doi.org/10.1021/am500398p | ACS Appl. Mater. Interfaces 2014, 6, 4560−4569

be broken when the particle is anisotropic in either geometry or interfacial property such as our dimers. Because both the tangential field and the induced charges are dependent on the applied field, the EHDF also scales with E_0^2.[53] This relationship was clearly illustrated in Figure 10a.

Although the EHDF is essentially an induced-charge electroosmosis along the electrode, there are some subtle differences between EHDF and ICEO on the particle. For example, ICEO around a dielectric particle is negligible. Although EHDF is initiated from the conducting substrate, it has impacts on both dielectric and metallic particles, as long as they are close to the substrate. Also, the emergence of the tangential field is different between EHDF and ICEO. In EHDF, the tangential field component arises from the polarization field of the particle's induced dipole. Therefore, the polarization coefficient K, especially its imaginary part K'' (which represents the phase lag between the dipole field and the applied field) is an important parameter in EHDF. On the basis of the theory of EHDF,[54] it can be further shown that the EHDF velocity near a spherical particle is

$$U_{\mathrm{EHDF}} \approx f\frac{K''\kappa D}{\omega}\frac{\varepsilon\varepsilon_0 E_0^2}{\mu} \tag{3}$$

where f is a prefactor that depends on the distance between the particle and the electrode and ω is the frequency. As can be seen from eq 3, when K'' is negative, the velocity is also negative, i.e., the solvent flows toward the particle, whereas it flows away from the particle when K'' is positive. Both the real and imaginary parts of the polarization coefficient K can be calculated on the basis of the standard electrokinetic model.[55] Figure 11a shows the K''/ω for both dielectric and metallic spheres of identical sizes. Within the frequency range of our interest, K'' is negative for the dielectric lobe and positive for the metallic lobe. Therefore, the EHDF is directed toward the dielectric lobe and is away from the platinum-coated lobe, as schematically illustrated in Figure 11b. Clearly, the net effect of the EHDF on the hybrid dimer is to push the dielectric lobe and to draw the Pt-coated lobe toward the right. On the contrary, the ICEO flow would push the metallic lobe (and the dimer) toward the left. Therefore, the net moving direction of the dimer would depend on the competition between EHDF and ICEO. When the EHDF velocity is larger than ICEO, the dimer would move with its metallic lobe orienting forward. The opposite orientation will be observed if ICEO flow is stronger than the EHDF. Since τ_p is ~15 kHz in deionized water (assuming $\kappa^{-1} \approx 150$ nm), the ICEO flow on the platinum-coated lobe is relatively constant for 400 Hz < ω < 2500 Hz. As shown in eq 3 and Figure 11a, the EHDF on the polystyrene lobe decreases with increasing frequency, and the EHDF on the platinum-coated lobe is almost a constant. Therefore, at low frequencies, the combined EHDF on both lobes is stronger than the ICEO, which pushes the dimer toward the platinum-coated lobe. As the frequency increases, the EHDF on the polystyrene lobe becomes weaker, which slows down the dimer propulsion. Combining eqs 2 and 3, we can calculate the EHDF velocities acting on both lobes and the ICEO velocity on the metallic lobe. The net velocity of the dimer at different frequencies is plotted by the solid line in Figure 10b. Our calculation fits the experimental data reasonably well.

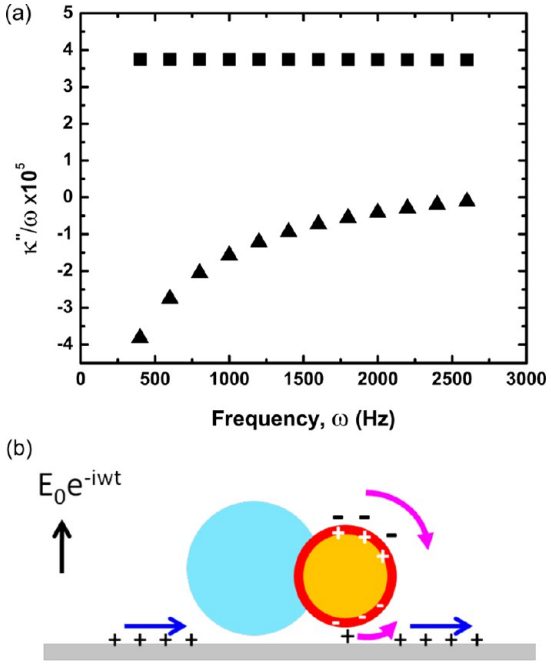

Figure 11. (a) K''/ω for dielectric (triangle) and metallic (square) spheres (R = 0.9 μm) as a function of the frequency ω. They are calculated based on the standard electrokinetic model.[55,17] (b) Schematics showing the competition between the EHDF (blue arrows) and ICEO (pink arrows) on the hybrid dimer. The EHDF pushes the dimer to the right, whereas the ICEO pushes the dimer to the left.

Because the density of the platinum coating on our dimers could have some variations due to the chemical synthesis method. For those dimers coated with dense layer of platinum, the ICEO could be still strong enough that its moving direction cannot be reversed by the EHDF. However, their velocities should be significantly reduced because of the opposite impact of the EHDF, which explains our observation that some dimers move with its dielectric lobe orienting forward but with much reduced velocities. At higher salt concentrations (e.g., 1×10^{-4} M KCl), the magnitudes of EHDF around the dielectric and platinum-coated lobes will be reduced by about one order of magnitude due to a much smaller K'', based on our calculation. Therefore, they are not strong enough to compete with the ICEO and change the propulsion direction of the dimers. Another interesting phenomena occurs around 2.2 kHz in DI water, where the ICEO is approximately balanced by EHDF on the metallic lobe and the dimer's velocity is approximately zero. Coincidently at this frequency, the dimer changes its orientation by aligning itself with the applied electric field, i.e., it stands up. Such an orientation change reintroduces the symmetry of ICEO and EHDF surrounding the (standing) particle. Therefore, the dimer stops moving when they stand on the substrate. Interestingly, we observe that whenever the Pt-PS dimer stands up, the platinum-coated lobe always points toward the substrate (see the Supporting Information, Movie 6). This could be resulted from the sum of the torques imposed by ICEO, EHDF, and the external electric fields. The competition between EHDF and ICEO on asymmetric particles can have many interesting effects and lead to some surprising results. More detailed analyses, which are beyond our scope here, will be presented in a separate paper.

3. CONCLUSIONS

We report a bulk-synthesis strategy to make metal–organic hybrid dimers with both geometric and interfacial anisotropy.

By changing the type of functional vinylsilanes in the cross-linked seed particles and the amount of styrene in the swelling stage, we can tune the geometric anisotropy such as the bond length $L/(R_1 + R_2)$ from 0.3 to 1 and the size ratio R_1/R_2 from 0.45 to 1. By taking advantage of the amine-metal complexation, gold nanoparticles can be coated selectively on the cross-linked lobe, forming metal−organic hybrid dimers. Dense metallic shells such as gold, silver, and platinum can be further grown on the gold-seeded lobe due to enhanced heterogeneous nucleation. Among various types of reducing agents, the chemical with a lower reduction speed (e.g., formaldehyde for gold/silver and ascorbic acid for platinum) can make hybrid dimers with excellent contrast in surface coating between two lobes. With the complementary difference in surface chemistry between the metallic and organic lobes, it is possible to further modify the interfacial properties on asymmetric particles, such as the hydrophobicity, surface charge, catalytic activity, etc. Such a synthetic platform will allow facile tuning of the geometric and interfacial anisotropy on a wide range of metal−organic hybrid dimers, which offers abundant opportunities to study their specific and synergistic impacts on self-assembly, multitasking and self-motile motors, colloidal emulsifiers, etc.

Once having synthesized the platinum-polystyrene dimers, we further investigate the self-propulsion of those particles under perpendicularly applied electric fields. In higher salt concentrations (e.g., 1×10^{-4} M KCl solution), the hybrid dimers exhibited both linear and circular motions. This is due to the significant contrast in the electric polarizability between metal-coated and polystyrene lobes, where the induced-charge electroosmotic flow surrounding the metal-coated lobe propels the dimer with its polystyrene lobe facing toward the moving direction. The same dimer, however, can move with the opposite orientation in deionized water, i.e., the dimer orients its metal-coated lobe toward the propelling direction. Although the velocities in both cases scale with the square of the applied field, their frequency dependence are rather different. We argue that an additional electroosmotic flow, the electrohydrodynamic flow arising from the induced charges along the conducting substrate, can also propel the dimer. Depending on both frequency and salt concentration, the competition between the electrohydrodynamic and the induced-charge electroosmosis can influence the orientation of the dimer during its propulsion. Interestingly, the propulsion speed of the dimer can be tuned by its orientation too. When it lies on the substrate, it moves due to the asymmetric EHD and ICEO flow. The flow asymmetry disappears when it stands on the substrate (i.e., aligning parallel to the applied field). Therefore, the synergistic effect of both geometric and interfacial anisotropy can be utilized to control both propulsion and orientation of colloidal dimers.

■ ASSOCIATED CONTENT

Supporting Information

The movies for the propulsion of hybrid dimers and the propulsion speeds of both symmetric and asymmetric PS-Pt dimers. This material is available free of charge via the Internet at http://pubs.acs.org/.

■ AUTHOR INFORMATION

Corresponding Author

*E-mail: ningwu@mines.edu.

Author Contributions

S.W., F.M., N.W. planned the research and designed the experiments. S. Wang synthesized the dimers and F. Ma performed experiments on the propulsion of dimers under electric fields. H. Zhao and N. Wu developed theoretical models to explain the experimental observations. All authors analyzed the results and wrote the manuscript. All authors have given approval to the final version of the manuscript.

Notes

The authors declare no competing financial interest.

■ ACKNOWLEDGMENTS

This work was supported by the start-up funds from Colorado School of Mines and National Science Foundation (CBET-1336893).

■ REFERENCES

(1) Sacanna, S.; Irvine, W. T. M.; Chaikin, P. M.; Pine, D. J. Lock and Key Colloids. *Nature* **2010**, *464*, 575−578.
(2) Nisisako, T.; Torii, T.; Takahashi, T.; Takizawa, Y. Synthesis of Monodisperse Bicolored Janus Particles with Electrical Anisotropy Using a Microfluidic Co-Flow System. *Adv. Mater.* **2006**, *18*, 1152−1156.
(3) Tanaka, T.; Okayama, M.; Minami, H.; Okubo, M. Dual Stimuli-Responsive "Mushroom-Like" Janus Polymer Particles as Particulate Surfactants. *Langmuir* **2010**, *0*, 11732−11736.
(4) Choi, J.; Zhao, Y.; Zhang, D.; Chien, S.; Lo, Y.-H. Patterned Fluorescent Particles as Nanoprobes for the Investigation of Molecular Interactions. *Nano Lett.* **2003**, *3*, 995−1000.
(5) Paxton, W. F.; Kistler, K. C.; Olmeda, C. C.; Sen, A.; St Angelo, S. K.; Cao, Y.; Mallouk, T. E.; Lammert, P. E.; Crespi, V. H. Catalytic Nanomotors: Autonomous Movement of Striped Nanorods. *J. Am. Chem. Soc.* **2004**, *126*, 13424−13431.
(6) Kagan, D.; Laocharoensuk, R.; Zimmerman, M.; Clawson, C.; Balasubramanian, S.; Kang, D.; Bishop, D.; Sattayasamitsathit, S.; Zhang, L.; Wang, J. Rapid Delivery of Drug Carriers Propelled and Navigated by Catalytic Nanoshuttles. *Small* **2010**, *6*, 2741−2747.
(7) Tong, L.; Wei, Q.; Wei, A.; Cheng, J.-X. Gold Nanorods as Contrast Agents for Biological Imaging: Optical Properties, Surface Conjugation and Photothermal Effects. *Photochem. Photobiol.* **2009**, *85*, 21−32.
(8) Wang, Y.; Wang, Y.; Breed, D. R.; Manoharan, V. N.; Feng, L.; Hollingsworth, A. D.; Weck, M.; Pine, D. J. Colloids with Valence and Specific Directional Bonding. *Nature* **2012**, *491*, 51−55.
(9) Perro, A.; Reculusa, S.; Ravaine, S.; Bourgeat-Lami, E.; Duguet, E. Design and Synthesis of Janus Micro- and Nanoparticles. *J. Mater. Chem.* **2005**, *15*, 3745−3760.
(10) Wilson, D. A.; Nolte, R. J. M.; Hest, J. C. M. Van Autonomous Movement of Platinum-Loaded Stomatocytes. *Nat. Chem.* **2012**, *4*, 268−274.
(11) Ke, H.; Ye, S.; Carroll, R. L.; Showalter, K. Motion Analysis of Self-Propelled Pt-Silica Particles in Hydrogen Peroxide Solutions. *J. Phys. Chem. A* **2010**, *114*, 5462−5467.
(12) Gibbs, J. G.; Zhao, Y. P. Autonomously Motile Catalytic Nanomotors by Bubble Propulsion. *Appl. Phys. Lett.* **2009**, *94*, 163104−3.
(13) Chang, S. T.; Paunov, V. N.; Petsev, D. N.; Velev, O. D. Remotely Powered Self-Propelling Particles and Micropumps Based on Miniature Diodes. *Nat. Mater.* **2007**, *6*, 235−240.
(14) Howse, J. R.; Jones, R. A. L.; Ryan, A. J.; Gough, T.; Vafabakhsh, R.; Golestanian, R. Self-Motile Colloidal Particles: From Directed Propulsion to Random Walk. *Phys. Rev. Lett.* **2007**, *99*, 048102−4.
(15) Anderson, J. L.; Prieve, D. C. Diffusiophoresis Caused by Gradients of Strongly Adsorbing Solutes. *Langmuir* **1991**, *7*, 403−406.
(16) Gangwal, S.; Cayre, O.; Bazant, M.; Velev, O. Induced-Charge Electrophoresis of Metallodielectric Particles. *Phys. Rev. Lett.* **2008**, *100*, 1−4.

(17) Squires, T. M.; Bazant, M. Z. Induced-Charge Electro-Osmosis. *J. Fluid Mech.* **2004**, *509*, 217−252.
(18) Squires, T. M.; Bazant, M. Z. Breaking Symmetries in Induced-Charge Electro-Osmosis and Electrophoresis. *J. Fluid Mech.* **2006**, *560*, 65−101.
(19) Liu, B.; Wei, W.; Qu, X.; Yang, Z. Janus Colloids Formed by Biphasic Grafting at a Pickering Emulsion Interface. *Angew. Chem., Int. Ed.* **2008**, *47*, 3973−3975.
(20) Liu, B.; Zhang, C.; Liu, J.; Qu, X.; Yang, Z. Janus Non-Spherical Colloids by Asymmetric Wet-Etching. *Chem. Commun.* **2009**, *0*, 3871−3873.
(21) Xing, S.; He, J.; Liu, X.; Chen, H. A Symmetry-Adapted Shell Transformation of Core-Shell Nanoparticles for Binary Nanoassembly. *Chem. Commun.* **2011**, *47*, 12533−12535.
(22) Perro, A.; Duguet, E.; Lambert, O.; Taveau, J.-C.; Bourgeat-Lami, E.; Ravaine, S. A Chemical Synthetic Route Towards "Colloidal Molecules. *Angew. Chem., Int. Ed.* **2009**, *48*, 361−365.
(23) Yu, H.; Chen, M.; Rice, P. M.; Wang, S. X.; White, R. L.; Sun, S. Dumbbell-Like Bifunctional Au-Fe3O4 Nanoparticles. *Nano Lett.* **2005**, *5*, 379−382.
(24) Shi, W.; Sahoo, Y.; Zeng, H.; Ding, Y.; Swihart, M. T.; Prasad, P. N. Anisotropic Growth of PbSe Nanocrystals on Au−Fe3O4 Hybrid Nanoparticles. *Adv. Mater.* **2006**, *18*, 1889−1894.
(25) Chen, T.; Yang, M.; Wang, X.; Tan, L. H.; Chen, H. Controlled Assembly of Eccentrically Encapsulated Gold Nanoparticles. *J. Am. Chem. Soc.* **2008**, *130*, 11858−11859.
(26) Ohnuma, A.; Cho, E. C.; Camargo, P. H. C.; Au, L.; Ohtani, B.; Xia, Y. A Facile Synthesis of Asymmetric Hybrid Colloidal Particles. *J. Am. Chem. Soc.* **2009**, *131*, 1352−1353.
(27) Zhang, C.; Liu, B.; Tang, C.; Liu, J.; Qu, X.; Li, J.; Yang, Z. Large Scale Synthesis of Janus Submicron Sized Colloids by Wet Etching Anisotropic Ones. *Chem. Commun.* **2010**, *46*, 4610−4612.
(28) Lu, W.; Chen, M.; Wu, L. One-Step Synthesis of Organic-Inorganic Hybrid Asymmetric Dimer Particles via Miniemulsion Polymerization and Functionalization with Silver. *J. Colloid Interface Sci.* **2008**, *328*, 98−102.
(29) Sheu, H. R.; El-Aasser, M. S.; Vanderhoff, J. W. Uniform Nonspherical Latex Particles as Model Interpenetrating Polymer Networks. *J. Polym. Sci., Part A: Polym. Chem.* **1990**, *28*, 653−667.
(30) Sheu, H. R.; El-Aasser, M. S.; Vanderhoff, J. W. Phase Separation in Polystyrene Latex Interpenetrating Polymer Networks. *J. Polym. Sci., Part A: Polym. Chem.* **1990**, *28*, 629−651.
(31) Kim, J.-W.; Larsen, R. J.; Weitz, D. A. Synthesis of Nonspherical Colloidal Particles with Anisotropic Properties. *J. Am. Chem. Soc.* **2006**, *128*, 14374−14377.
(32) Tang, C.; Zhang, C.; Liu, J.; Qu, X.; Li, J.; Yang, Z. Large Scale Synthesis of Janus Submicrometer Sized Colloids by Seeded Emulsion Polymerization. *Macromolecules* **2010**, *43*, 5114−5120.
(33) Kim, J.-W.; Lee, D.; Shum, H. C.; Weitz, D. A. Colloid Surfactants for Emulsion Stabilization. *Adv. Mater.* **2008**, *20*, 3239−3243.
(34) Park, J.-G.; Forster, J. D.; Dufresne, E. R. High-Yield Synthesis of Monodisperse Dumbbell-Shaped Polymer Nanoparticles. *J. Am. Chem. Soc.* **2010**, *132*, 5960−5961.
(35) Yoon, K.; Lee, D.; Kim, J. W.; Kim, J.; Weitz, D. A. Asymmetric Functionalization of Colloidal Dimer Particles with Gold Nanoparticles. *Chem. Commun.* **2012**, 9056−9058.
(36) Mock, E. B.; Bruyn, H.; De Hawkett, B. S.; Gilbert, R. G.; Zukoski, C. F. Synthesis of Anisotropic Nanoparticles by Seeded Emulsion Polymerization. *Langmuir* **2006**, *22*, 4037−4043.
(37) Mock, E. B.; Zukoski, C. F. Emulsion Polymerization Routes to Chemically Anisotropic Particles. *Langmuir* **2010**, *26*, 13747−13750.
(38) Plueddemann, E. P. *Silane Coupling Agents*; Springer: New York, 1982.
(39) Graf, C.; Blaaderen, A. Van Metallodielectric Colloidal Core−Shell Particles for Photonic Applications. *Langmuir* **2002**, *18*, 524−534.
(40) Xue, J.; Wang, C.; Ma, Z. A Facile Method to Prepare a Series of SiO_2@Au Core/shell Structured Nanoparticles. *Mater. Chem. Phys.* **2007**, *105*, 419−425.
(41) Zhang, F.; Cao, L.; Yang, W. Preparation of Monodisperse and Anion-Charged Polystyrene Microspheres Stabilized with Polymerizable Sodium Styrene Sulfonate by Dispersion Polymerization. *Mater. Sci.* **2010**, *211*, 744−751.
(42) Turkevich, J.; Stevenson, P. C.; Hillier, J. A Study of the Nucleation and Growth Processes in the Synthesis of Colloidal Gold. *Discuss. Faraday Soc.* **1951**, *11*, 55−75.
(43) Abramoff, M. D.; Magalhães, P. J.; Ram, S. J. Image Processing with ImageJ. *Biophotonics Int.* **2004**, *11*, 36−42.
(44) Feng, Y.; He, J.; Wang, H.; Tay, Y. Y.; Sun, H.; Zhu, L.; Chen, H. An Unconventional Role of Ligand in Continuously Tuning of Metal-Metal Interfacial Strain. *J. Am. Chem. Soc.* **2012**, *134*, 2004−7.
(45) Jensen, T. R.; Malinsky, M. D.; Haynes, C. L.; Duyne, R. P. Van Nanosphere Lithography: Tunable Localized Surface Plasmon Resonance Spectra of Silver Nanoparticles. *J. Phys. Chem. B* **2000**, *104*, 10549−10556.
(46) Yong, K.-T.; Sahoo, Y.; Swihart, M. T.; Prasad, P. N. Synthesis and Plasmonic Properties of Silver and Gold Nanoshells on Polystyrene Cores of Different Size and of Gold−Silver Core−Shell Nanostructures. *Colloids Surfaces., A* **2006**, *290*, 89−105.
(47) Montero, M. A.; Chialvo, M. R. G. de; Chialvo, A. C. Electrocatalytic Activity of Core−Shell Au@Pt Nanoparticles for the Hydrogen Oxidation Reaction. *Int. J. Hydrogen Energy* **2011**, *36*, 3811−3816.
(48) Li, J.-F.; Yang, Z.-L.; Ren, B.; Liu, G.-K.; Fang, P.-P.; Jiang, Y.-X.; Wu, D.-Y.; Tian, Z.-Q. Surface-Enhanced Raman Spectroscopy Using Gold-Core Platinum-Shell Nanoparticle Film Electrodes: Toward a Versatile Vibrational Strategy for Electrochemical Interfaces. *Langmuir* **2006**, *22*, 10372−10379.
(49) Lu, L.; Sun, G.; Xi, S.; Wang, H.; Zhang, H.; Wang, T.; Zhou, X. A Colloidal Templating Method To Hollow Bimetallic Nanostructures. *Langmuir* **2003**, *19*, 3074−3077.
(50) Levitan, J. A.; Devasenathipathy, S.; Studer, V.; Ben, Y.; Thorsen, T.; Squires, T. M.; Bazant, M. Z. Experimental Observation of Induced-Charge Electro-Osmosis Around a Metal Wire in a Microchannel. *Colloids Surfaces., A* **2005**, *267*, 122−132.
(51) Trau, M.; Saville, D. A.; Aksay, I. A. Field-Induced Layering of Colloidal Crystals. *Science* **1996**, *272*, 706−709.
(52) Trau, M.; Saville, D. a; Aksay, I. a Assembly of Colloidal Crystals at Electrode Interfaces. *Langmuir* **1997**, *13*, 6375−6381.
(53) Ristenpart, W. D.; Aksay, I. A.; Saville, D. A. Assembly of Colloidal Aggregates by Electrohydrodynamic Flow: Kinetic Experiments and Scaling Analysis. *Phys. Rev. E* **2004**, *69*, 021405.
(54) Ristenpart, W. D.; Aksay, I. A.; Saville, D. A. Electrohydrodynamic Flow Around a Colloidal Particle Near an Electrode with an Oscillating Potential. *J. Fluid Mech.* **2007**, *575*, 83−109.
(55) Zhao, H. Double-Layer Polarization of a Non-Conducting Particle in an Alternating Current Field with Applications to Dielectrophoresis. *Electrophoresis* **2011**, *32*, 2232.